Effects of Side-Wall Grooves on Transmission Characteristics of Suspended Striplines

EIKICHI YAMASHITA, FELLOW, IEEE, BAI YI WANG, KAZUHIKO ATSUKI, AND KE REN LI

Abstract—**The use of suspended striplines is becoming an important transmission-line technique at millimeter wavelengths because of low attenuation, weak dispersion, and various merits in manufacturing processes. This paper estimates the effects of side-wall grooves of these lines on transmission characteristics within the TEM wave approximation.**

I. Introduction

SUSPENDED STRIPLINES (SSL's) have become very useful for millimeter-wave transmission recently (as discussed in the workshop on SSL filters in the 1984 International Microwave Symposium) because of their low attenuation, weak dispersion, and moderate wavelength reduction factor compared with microstrip lines, and various merits in manufacturing processes. The planar configuration also makes SSL's suitable for integration into millimeter-wave systems [1].

The transmission characteristics of SSL's as shown in Fig. 1 have already been analyzed both for thin-strip cases [2] and thick-strip cases [3]. However, effects of side-wall grooves, which have recently been employed in practical SSL's to support substrates mechanically, as shown in Fig. 2, have not been estimated theoretically, except a transverse resonance analysis [4] in which the cutoff frequency of the TE_{10} type mode has been calculated. In the case of finlines, the effects of grooves on hybrid-mode transmission have been estimated by using the mode-matching method [5]. The applications and technology of suspended striplines at millimeter wavelengths have been well described in other literature [6], [7].

This paper shows the method and results of the quantitative analysis of such effects, particularly on the characteristic impedance and wavelength reduction factor.

II. Method of Analysis

The present analysis of transmission characteristics of SSL's with side-wall grooves is carried out within the TEM-wave approximation since the weak dispersion of the dominant mode is expected because of the existence of two air regions. The past methods using Green's function [2], [3] cannot be applied to this structure because of its irregular shape.

Manuscript received March 19, 1985; revised June 25, 1985.

The authors are with the University of Electro-Communications, Chofu-shi, Tokyo, Japan 182.

The solution of Laplace's equation is first assumed for each of the three regions in Fig. 2. The strip conductor is assumed to be infinitely thin. Potential functions which satisfy boundary conditions at the surrounding conductor surface can be written in the form of Fourier series as

$$\phi_1(x,y)=\sum_{n=1,3,5}^{\infty} A_n \sinh\left(\frac{n\pi y}{a}\right)\cos\left(\frac{n\pi x}{a}\right) \quad \left(|x|\leqslant\frac{a}{2},\ 0\leqslant y\leqslant h_1\right) \tag{1}$$

$$\phi_2(x,y)=\sum_{n=1,3,5}^{\infty}\left[B_n\sinh\left(\frac{n\pi y}{a+2d}\right)+C_n\cosh\left(\frac{n\pi y}{a+2d}\right)\right]\cdot\cos\left(\frac{n\pi x}{a+2d}\right) \quad \left(|x|\leqslant\frac{a}{2}+d,\ h_1\leqslant y\leqslant h_1+h_2\right) \tag{2}$$

$$\phi_3(x,y)=\sum_{n=1,3,5}^{\infty} D_n\sinh\left[\frac{n\pi(b-y)}{a}\right]\cos\left(\frac{n\pi x}{a}\right) \quad \left(|x|\leqslant\frac{a}{2},\ h_1+h_2\leqslant y\leqslant b\right). \tag{3}$$

When potential functions at $y=h_1-0$, $y=h_1+0$, $y=h_1+h_2-0$, and $y=h_1+h_2+0$ are given by $f_1(x)$, $f_2(x)$, $f_3(x)$, and $f_4(x)$, respectively, (1)–(3) lead to the Fourier series expansions of these functions. The Fourier coefficients A_n, B_n, C_n, and D_n are uniquely determined after knowing these functions. The variational method is used to find the form of these functions.

We use the fact that the total electric-field energy W of this structure per unit length is given by

$$W=\frac{1}{2}\sum_{i=1}^{3}\epsilon_i\iint_{S_i}\left[\left(\frac{\partial\phi_i}{\partial x}\right)^2+\left(\frac{\partial\phi_i}{\partial y}\right)^2\right]dx\,dy \tag{4}$$

where S_i $(i=1,2,3)$ denotes the cross-sectional area and ϵ_i $(i=1,2,3)$ the dielectric constant of the region i. This energy can be minimized by varying the form of the above potential functions at $y=h_1$ and $y=h_1+h_2$ as trial functions. The minimized energy $W_{\min}$ is related to the line capacitance C by

$$W_{\min}=\frac{1}{2}CV^2 \tag{5}$$

0018-9480/85/1200-1323$01.00 ©1985 IEEE

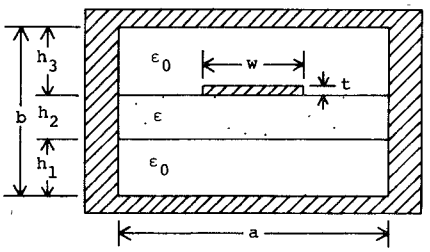

Fig. 1. Suspended striplines without side-wall grooves.

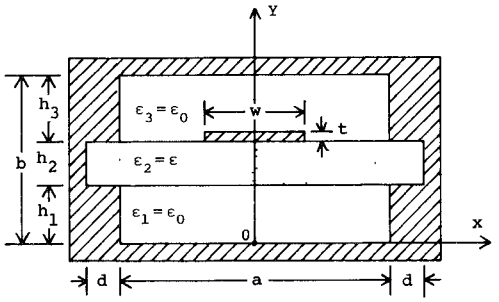

Fig. 2. Suspended striplines with side-wall grooves.

where V denotes the potential difference between the strip and wall conductor. Then, the characteristic impedance Z and the wavelength reduction factor λ/λ_0 within the TEM-wave approximation are given by

$$Z = \frac{1}{v_0\sqrt{CC_o}} \tag{6}$$

$$\frac{\lambda}{\lambda_0} = \sqrt{\frac{C_o}{C}} \tag{7}$$

where v_0 is the velocity of light in vacuum and C_0 is the line capacitance for the case $\epsilon_1 = \epsilon_2 = \epsilon_3 = \epsilon_0$.

III. Trial Functions and Variational Formulation

Because of the symmetry of the structure, the potential functions have also even symmetry, and only one half of the structure has to be treated. The above four functions in the right half are mutually related as

$$f_1(x) = f_2(x) = f(x) \quad \left(0 \leqslant x \leqslant \frac{a}{2},\ y = h_1 - 0\right) \tag{8}$$

$$f_2(x) = 0 \quad \left(\frac{a}{2} \leqslant x \leqslant \frac{a}{2} + d,\ y = h_1 + 0\right) \tag{9}$$

$$f_3(x) = f_4(x) = g(x) \quad \left(0 \leqslant x \leqslant \frac{a}{2},\ y = h_1 + h_2 - 0\right) \tag{10}$$

$$f_3(x) = 0 \quad \left(\frac{a}{2} \leqslant x \leqslant \frac{a}{2} + d,\ y = h_1 + h_2 + 0\right). \tag{11}$$

Applying (8)–(11) to (1)–(3), we obtain the Fourier series whose coefficients are given by

$$A_n = \frac{4}{a\sinh\left(\frac{n\pi h_1}{a}\right)} \int_0^{a/2} f(x)\cos\left(\frac{n\pi x}{a}\right) dx \tag{12}$$

$$B_n = \frac{4}{(a+2d)\sinh\left(\frac{n\pi h_2}{a+2d}\right)} \left[\cosh\left(\frac{n\pi h_1}{a+2d}\right) \cdot \int_0^{a/2} g(x)\cos\left(\frac{n\pi x}{a+2d}\right) dx - \cosh\left[\frac{n\pi(h_1+h_2)}{a+2d}\right] \cdot \int_0^{a/2} f(x)\cos\left(\frac{n\pi x}{a+2d}\right) dx\right] \tag{13}$$

$$C_n = \frac{4}{(a+2d)\sinh\left(\frac{n\pi h_2}{a+2d}\right)} \left[-\sinh\left(\frac{n\pi h_1}{a+2d}\right) \cdot \int_0^{a/2} g(x)\cos\left(\frac{n\pi x}{a+2d}\right) dx + \sinh\left[\frac{n\pi(h_1+h_2)}{a+2d}\right] \cdot \int_0^{a/2} f(x)\cos\left(\frac{n\pi x}{a+2d}\right) dx\right] \tag{14}$$

$$D_n = \frac{4}{a\sinh\left(\frac{n\pi h_3}{a}\right)} \int_0^{a/2} g(x)\cos\left(\frac{n\pi x}{a}\right) dx. \tag{15}$$

Now, we choose the first-order spline function (or the polygonal line function) as trial functions to express $f(x)$ and $g(x)$ as given below, and as shown in Fig. 3, because the spline function has a simple form and is useful in approximating complicated curves

$$f(x) = \sum_{i=0}^{m_1} F_i(x) \tag{16}$$

$$g(x) = \sum_{j=0}^{m_2} G_j(x) \tag{17}$$

where

$$F_i(x) = \begin{cases} \dfrac{p_{i+1} - p_i}{a_{i+1} - a_i} x + \dfrac{p_i a_{i+1} - p_{i+1} a_i}{a_{i+1} - a_i} \\ \qquad (a_i \leqslant x \leqslant a_{i+1}) \\ 0 \quad \text{(elsewhere)} \end{cases} \tag{18}$$

$$G_j(x) = \begin{cases} \dfrac{q_{j+1} - q_j}{b_{j+1} - b_j} x + \dfrac{q_j b_{j+1} - q_{j+1} b_j}{b_{j+1} - b_j} \\ \qquad (b_j \leqslant x \leqslant b_{j+1}) \\ 0 \quad \text{(elsewhere)} \end{cases} \tag{19}$$

and the values of knot potentials of the trial function are denoted by p_i $(i = 0,1,\cdots,m_1+1)$ for $f(x)$, and q_j $(j = 0,1,\cdots,m_2+1)$ for $g(x)$ at the knot positions a_i $(i = 0,1,\cdots,m_1+1)$ and b_j $(j = 0,1,\cdots,m_2+1)$, respectively.

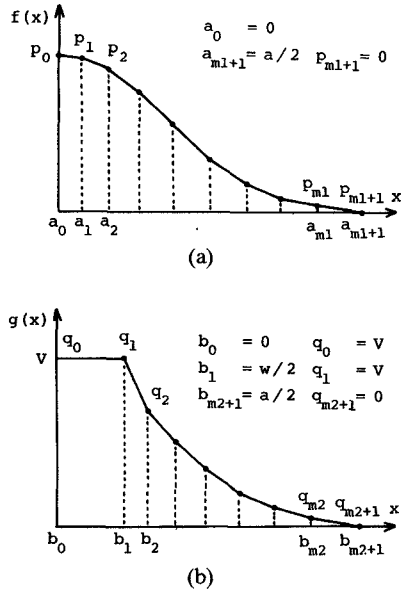

Fig. 3. The form of trial functions. (a) The first-order spline function as the trial function for $f(x)$. (b) The first-order spline function as the trial function for $g(x)$.

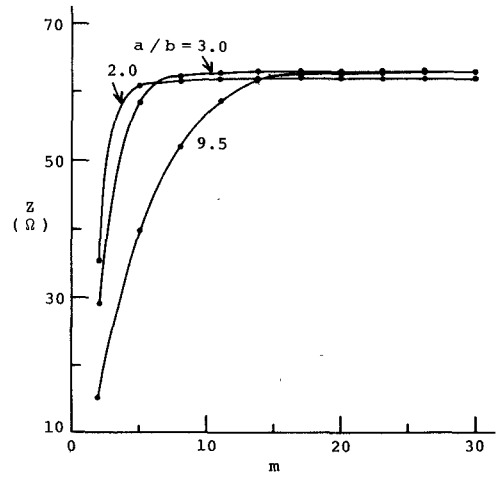

Fig. 4. The numerical convergence property of the characteristic impedance. $w/b = 1.0$, $h_1/b = 0.4$, $h_2/b = 0.2$, $h_3/b = 0.4$, $t = d = 0$, $\epsilon^* = 1.0$.

The total electric-field energy after the integration (4) is given by

$$W = \sum_{i=0}^{m_1}\sum_{k=0}^{m_1} \alpha_{ik} p_i p_k + \sum_{j=0}^{m_2}\sum_{k=0}^{m_2} \beta_{jk} q_j q_k - 2\sum_{i=0}^{m_1}\sum_{j=0}^{m_2} \gamma_{ij} p_i q_j \quad (20)$$

where symbols α_{ik}, β_{jk}, and γ_{ij} are defined in the Appendix.

This energy expression includes a group of knot potentials (p_0, $p_1, \cdots, p_{m1}$, q_2, $q_3, \cdots,$ and q_{m2}) as new variables and remaining knot potentials (p_{m1+1}, q_0, q_1, and q_{m2+1}) as constants. These new variables are adjusted to satisfy the following conditions to obtain the minimum of W:

$$\frac{\partial W}{\partial p_i} = 0 \qquad (i = 0,1,\cdots,m_1) \quad (21)$$

$$\frac{\partial W}{\partial q_j} = 0 \qquad (j = 2,3,\cdots,m_2). \quad (22)$$

By imposing these conditions on the energy expression (20), we obtain a set of linear, simultaneous, inhomogeneous equations as shown below which are the final equations to be solved on a computer

$$\sum_{k=0}^{m_1} \alpha_{ik} p_k - \sum_{j=2}^{m_2} \gamma_{ij} q_j = \sum_{j=0}^{1} \gamma_{ij} q_j \qquad (i = 0,1,\cdots,m_1) \quad (23)$$

$$\sum_{i=0}^{m_1} \gamma_{ij} p_i - \sum_{k=2}^{m_2} \beta_{jk} q_k = \sum_{k=0}^{1} \beta_{jk} q_k \qquad (j = 2,3,\cdots,m_2). \quad (24)$$

Since the knot potentials are known after solving these equations, the minimum value of the electric-field energy is found by substituting these values into (20).

V. Numerical Processing and Accuracy

The numbers of the knots of the trial function m_1 and m_2 play an important role in determining the required time for computation and accuracy. Since $g(x)$ changes sharply compared with $f(x)$, m_2 is necessarily larger than m_1. m_1 and m_2 can be minimized by taking the following measures.

1) The sizes of m_1 and m_2 are increased when those of $a/2b$ and $(a-w)/b$ are increased, respectively.

2) The knots of the spline function for $g(x)$ near the strip conductor are narrowly spaced to represent potential curves precisely. Fig. 4 shows the convergence property of the impedance values for increasing the sum of the two values $m = m_1 + m_2$. The effect of the number of the Fourier series terms N is less important when N is larger than 100. Typical values of these numbers in the present analysis are: $m_1 = 7$, $m_2 = 13$, and $N = 100$.

The accuracy of calculated transmission parameters can be examined by comparing numerical results for the case of $d = 0$ by the present method with those by the previous method [2]. Fig. 5 indicates that both methods result in good agreement with the discrepancy by approximately 0.1 percent. This agreement is due to the fact that λ/λ_0 is expressed by $\sqrt{C_0/C}$, in which capacitance errors are mostly cancelled.

Fig. 6, on the other hand, indicates that there is a discrepancy of about 2 percent between the impedance values calculated by the two methods. This is naturally attributed to the expression of the characteristic impedance inversely proportional to $\sqrt{C_0 C}$. However, because of the nature of the present and the previous variational method, it can be stated that the exact values of the characteristic impedance exist between these two curves. The time required for computing a set of impedance and the wave-

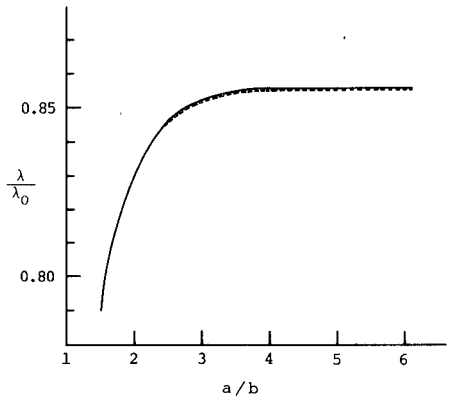

Fig. 5. A comparison of λ/λ_0 values by the present method (solid line) with those by the previous method (dashed line) for $d=0$. $w/b=1.0$, $h_1/b=0.4$, $h_2/b=0.2$, $h_3/b=0.4$, $t=d=0$, $\epsilon^*=3.78$.

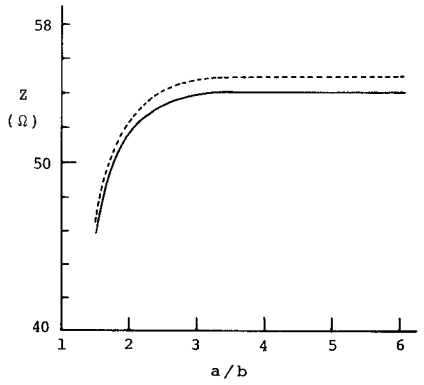

Fig. 6. A comparison of Z values by the present method (solid line) with those by the previous method (dashed line) for $d=0$. $w/b=1.0$, $h_1/b=0.4$, $h_2/b=0.2$, $h_3/b=0.4$, $t=d=0$, $\epsilon^*=3.78$.

length reduction factor was about 1 s on a HITAC-M180 computer.

VI. Numerical Results

Since the common values of the characteristic impedance are 50 Ω and 75 Ω, the structural dimensions of the SSL's in this paper are also selected by considering these values. Relatively high walls are treated in order to see the strong effects of side-wall grooves. For Duroid (the dielectric constant $\epsilon^*=2.22$) used as substrates, the following dimensions are used:

$$a/b=1.0 \quad h_1/b=0.4 \quad h_2/b=0.2 \quad h_3/b=0.4$$
$$t=0.0 \quad w/b=0.2\sim 0.9 \quad d/b=0.0\sim 0.5.$$

The results of numerical calculations are shown in Figs. 7 and 8. When the depth of grooves is increased, the characteristic impedance and wavelength reduction factor are also increased rapidly but eventually no more effects are observed in the region of deep grooves. The flatness of these curves is important since it assures us the exactness of our method. Because groove effects are significant in the range of small d, these can not be neglected when precise

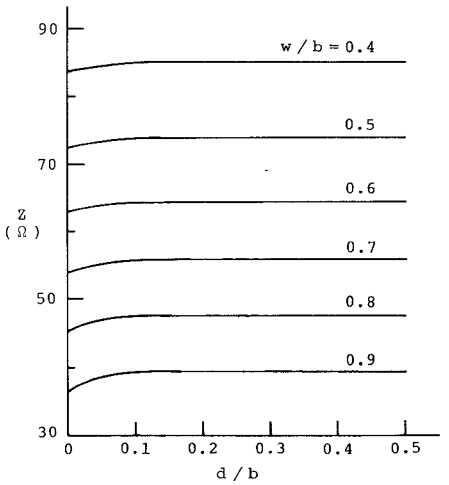

Fig. 7. Side-wall groove effects on the characteristic impedance Z. $a/b=1.0$, $h_1/b=0.4$, $h_2/b=0.2$, $h_3/b=0.4$, $t=0$, $\epsilon^*=2.22$.

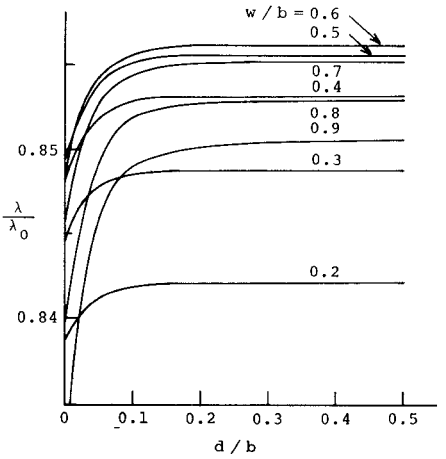

Fig. 8. Side-wall groove effects on the wavelength reduction factor λ/λ_0. $a/b=1.0$, $h_1/b=0.4$, $h_2/b=0.2$, $h_3/b=0.4$, $t=0$, $\epsilon^*=2.22$.

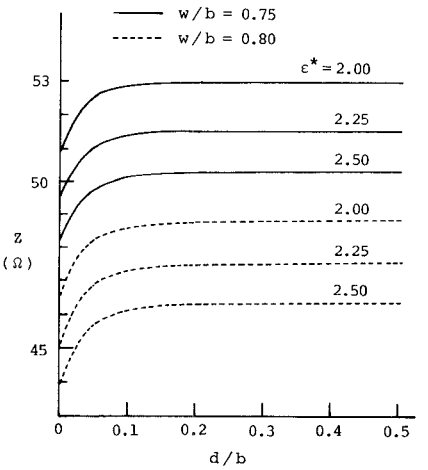

Fig. 9. Side-wall groove effects on the characteristic impedance for substrates of various dielectric constants. $a/b=1.0$, $h_1/b=0.4$, $h_2/b=0.2$, $h_3/b=0.4$, $t=0$.

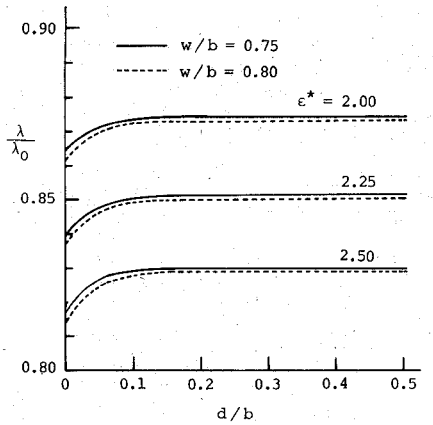

Fig. 10. Side-wall groove effects on the wavelength reduction factor for substrates of various dielectric constants. $a/b=1.0$, $h_1/b=0.4$, $h_2/b=0.2$, $h_3/b=0.4$, $t=0$.

filters are designed. In order to avoid these effects, very low side-walls ($b \ll a$) must be employed. However, it should be noted that the width a also determines the lowest cutoff frequency. Figs. 9 and 10 show the effects of the grooves on transmission characteristics with the dielectric constant of the substrate as parameters.

This method of analysis is simple and efficient in numerical computation, and can be applied to a variety of planar configurations as shown in Fig. 11.

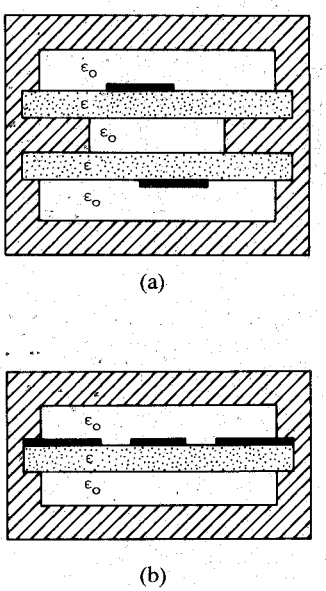

Fig. 11. Possible generalized structures for applying the present analysis method. (a) Coplanar SSL's. (b) SSL couplers.

APPENDIX

The symbols in the energy expression (20) are defined as follows:

$$\alpha_{ik}=\epsilon_1\sum_{n=1,3,5}^{\infty}\frac{4}{n\pi\tanh\left(\frac{n\pi h_1}{a}\right)}K_n(a_i,a)K_n(a_k,a)+\epsilon_2\sum_{n=1,3,5}^{\infty}\frac{4}{n\pi\tanh\left(\frac{n\pi h_2}{a+2d}\right)}\cdot K_n(a_i,a+2d)K_n(a_k,a+2d) \quad \text{(A1)}$$

$$\beta_{jk}=\epsilon_3\sum_{n=1,3,5}^{\infty}\frac{4}{n\pi\tanh\left(\frac{n\pi h_3}{a}\right)}K_n(b_j,a)K_n(b_k,a)+\epsilon_2\sum_{n=1,3,5}^{\infty}\frac{4}{n\pi\tanh\left(\frac{n\pi h_2}{a+2d}\right)}\cdot K_n(b_j,a+2d)K_n(b_k,a+2d) \quad \text{(A2)}$$

$$\gamma_{ij}=\epsilon_2\sum_{n=1,3,5}^{\infty}\frac{4}{n\pi\sinh\left(\frac{n\pi h_2}{a+2d}\right)}\cdot K_n(a_i,a+2d)K_n(b_j,a+2d) \quad \text{(A3)}$$

where

$$K_n(x_i,A)=\cos\left(\frac{n\pi x_i}{A}\right)\cdot\left[\frac{2}{R_i}\left(\sin\frac{R_i}{2}\right)^2+\frac{2}{R_{i+1}}\left(\sin\frac{R_{i+1}}{2}\right)^2\right]+\sin\left(\frac{n\pi x_i}{A}\right)\cdot\left[-\frac{1}{R_i}\sin R_i+\frac{1}{R_{i+1}}\sin R_{i+1}\right] \quad \text{(A4)}$$

$$R_i=\frac{n\pi(x_i-x_{i-1})}{A}. \quad \text{(A5)}$$

ACKNOWLEDGMENT

The authors thank Dr. Y. Suzuki for his helpful comments.

REFERENCES

[1] M. H. Arain, "A 94 GHz suspended stripline circulator," in *1984 IEEE MTT-S Symp. Dig.*, pp. 78–79.
[2] E. Yamashita and K. Atsuki, "Strip lines with rectangular outer conductor and three dielectric layers," *IEEE Trans. Microwave Theory Tech.*, vol. MTT-18, pp. 238–242, May 1970.
[3] K. Atsuki and E. Yamashita, "Analytical method for transmission lines with thick-strip conductor, multi-dielectric layers, and shielding conductor," *IECE Japan*, vol. 53-B, pp. 322–328, June 1970.
[4] S. B. Cohn and G. D. Osterhues, "A more accurate model of the TE_{10} – type waveguide mode in suspended substrate," *IEEE Trans. Microwave Theory Tech.*, vol. MTT-30, pp. 293–294, Mar. 1982.
[5] A. Beyer, "Analysis of the characteristics of an earthed finline," *IEEE Trans. Microwave Theory Tech.*, vol. MTT-29, 676–680, July 1981.
[6] C. Chao, A. Contolatis, S. A. Jamison, and P. E. Bauhahn, "*Ka*-band monolithic GaAs balanced mixers," *IEEE Trans. Microwave Theory Tech.*, vol. MTT-31, pp. 11–15, Jan. 1983.
[7] R. S. Tahim, G. M. Hayashibara, and K. Chang, "Design and performance of *W*-band broad-band integrated circuit mixers," *IEEE Trans. Microwave Theory Tech.*, vol. MTT–31, pp. 277–283, Mar. 1983.

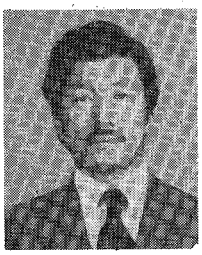

Eikichi Yamashita (M'66–SM'79–F'84) was born in Tokyo, Japan, on February 4, 1933. He received the B.S. degree from the University of Electro-Communications, Tokyo, Japan, and the M. S. and Ph.D. degrees from the University of Illinois, Urbana, all in electrical engineering, in 1956, 1963, and 1966, respectively.

From 1956 to 1964, he was a Member of the Research Staff on millimeter-wave engineering at the Electrotechnical Laboratory, Tokyo, Japan. While on leave from 1961 to 1963 and from 1964 to 1966, he studied solid-state devices in the millimeter-wave region at the Electro-Physics Laboratory, University of Illinois. From 1966 to 1967, he was with the Antenna Laboratory, University of Illinois. He became an Associate Professor in 1967 and Professor in 1977 in the Department of Applied electronics, the University of Electro-Communications, Tokyo, Japan. His research work since 1956 has been on microstrip transmission lines, suspended striplines, wave propagation in a gaseous plasma, pyroelectric-effect detectors in the submillimeter-wave region, tunnel-diode oscillators, wide-band laser modulators, and various types of optical fibers.

Dr. Yamashita is a member of the Institute of Electronics and Communication Engineers of Japan and Sigma Xi.

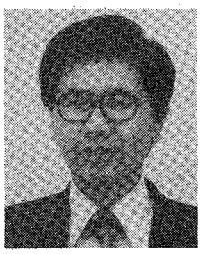

Kazuhiko Atsuki was born in Tokyo, Japan, on November 2, 1942. He received the B.S. and M.S. degrees from the University of Electro-Communications, Tokyo, Japan, and the Dr. Eng. degree from Tokyo University, Tokyo, Japan, all in electrical engineering, in 1965, 1967, and 1979, respectively.

He became Research Assistant in 1967, Instructor in 1979, and in 1982 Assistant Professor in the Department of Applied Electronics, the University of Electro-Communications, Tokyo, Japan. He has been studying switching transistors, microstrip transmission lines, wide-band laser modulators, and optical fibers.

Dr. Atsuki is a member of the Institute of Electronics and Communication Engineers of Japan.

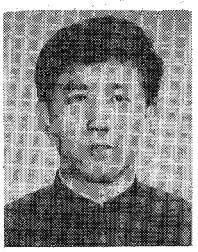

Bai Yi Wang was born in Shan Xi, China, on June 11, 1954. He received the B.S. degree from the Beijing Institute of Posts and Telecommunications, China, in 1978.

He has been an assistant in the Physics Department, the Beijing Institute of Posts and Telecommunications, since 1978. He is now on leave to study analysis methods for microwave transmission lines as a visiting Researcher at the University of Electro-Communications, Tokyo, Japan.

Ke Ren Li was born in Jiang Su, China, on June 22, 1962. He received the B.S. degree from the Nanjing Institute of Technology, China, in July, 1983.

He is presently a graduate student at the University of Electro-Communications, Tokyo, Japan. His field of interest is the characterization of microwave transmission lines and optical fibers.